Qualitative explanation for the Schäfer-Hubert effect: A boundary effect at the crossroads of magneto-optics and near-field optics

I. Banno*

Interdisciplinary Graduate School of Medicine and Engineering, University of Yamanashi, 4-3-11 Takeda, Kofu, Yamanashi 400-8511, Japan

(Received 2 September 2007; revised manuscript received 16 January 2008; published 7 March 2008)

I present a simple theoretical interpretation of an anomalous magneto-optical effect at the domain boundary. This effect was discovered by Schäfer and Hubert [Phys. Status Solidi A **118**, 271 (1990)] but was not supported by a clear physical explanation. From a familiar dielectric law, I derive the boundary magneto-optical effect concurrently with the bulk magneto-optical effect, i.e., the Faraday-Kerr effect. This boundary effect originates in the boundary charge density and is identified as the Schäfer-Hubert effect, based on a comparison of my theory and experimental results. Furthermore, I demonstrate that the Schäfer-Hubert effect predominates over the Faraday-Kerr effect and will be observed in the near field of a system with small-scale domains.

DOI: 10.1103/PhysRevA.77.033818 PACS number(s): 42.25.Gy, 78.20.Ls, 78.20.Bh, 68.37.Uv

I. INTRODUCTION

The magneto-optical effect (MOE) was discovered by Faraday in 1845 [1] and is used for optical sensing of magnetic fields. In a storage system using magnetic media, the MOE can be used to read out signals; see [2] for a review. The optical detection of small-scale magnetic domains is required for high bit-density magneto-optical (MO) storage. However, the domain size is diffraction limited, that is, if the domain size is smaller than the order of the light wavelength, then the partial fields scattered by the neighboring domains interfere and cannot be distinguished in far-field observation. To achieve higher bit density in the face of the diffraction limit, a near-field optical technique is essential for all types of optical storage including MO storage. If the observation point is sufficiently near the domains, the partial fields do not interfere and can be distinguished. Studies in this direction have continued since the pioneering study of Betzig *et al.* [3], who used a near-field optical microscope to observe magnetic domains on a small scale. Nevertheless, in the present state of the art, the bit density of MO and other types of optical storage is much less than that of hard disks. This is due to the technical difficulty and poor cost performance of near-field detectors, and perhaps a lack of fundamental knowledge about the boundary MOE discussed in this paper.

The importance of the boundary MOE in a small-scale system can be understood from the following fundamental concept of physics, one that is not well recognized in optics: The boundary effect, if it exists, predominates over the bulk effect in a small-scale structure, while the opposite is true for a large-scale structure. Considering that near-field optics permit the observation of a small-scale system, the above principle indicates that the boundary MOE is situated at the crossroads of magneto-optics and near-field optics. From this perspective, I provide evidence of the boundary MOE. Among various optical effects, the MOE is remarkable. The bulk effect, i.e., the Faraday-Kerr (FK) effect [12] can be extinguished under certain configurations, so that the boundary MOE is detectable even in a large-scale system without using near-field optical techniques. It was under such conditions in 1990 that Schäfer and Hubert discovered an anomalous MOE on the domain boundary using Kerr optics [4]. However, the Schäfer-Hubert (SH) effect was not supported by a clear physical explanation, although some theoretical studies for the gradient effect of magnetization have been developed, as shown in Sec. II.

The purpose of this paper is to give a simple theoretical interpretation of the SH effect as evidence of a boundary MOE originating from boundary charge density. The outline of this paper is as follows. Section II gives a review of experimental and theoretical pioneering studies related to the SH effect. In Sec. III, I develop my theory based on a familiar dielectric law, and this leads to a boundary MOE concurrently with the bulk MOE. The bulk MOE is the FK effect, and I show in Sec. IV by comparing my theory to the experimental results, that the boundary MOE is the SH effect. I compare my theory with other theories in Sec. V. In Sec. VI, I predict that the SH effect is dominant and detectable in the near field of a system with small-scale domains. Section VII is the summary. Two appendixes are provided. In Appendix A, I explain that the singularity of the boundary charge density appearing in my theory is responsible for Maxwell's boundary conditions (MBCs). Appendix B gives the derivation details of a certain formula.

The present theoretical scheme implies a general rule in optics that corresponding to every known bulk effect, there exists a boundary effect driven by boundary charge density. In another presentation, it will be shown that in general, such boundary optical effects including the boundary MOE are dominant in a system of near-field optics.

II. SCHÄFER-HUBERT EFFECT

In this section, I introduce the experimental and theoretical results of pioneering studies related to the SH effect. In 1990, Schäfer and Hubert [4] first observed an anomalous MOE of the domain boundary using Kerr optics, and one of

*banno@yamanashi.ac.jp

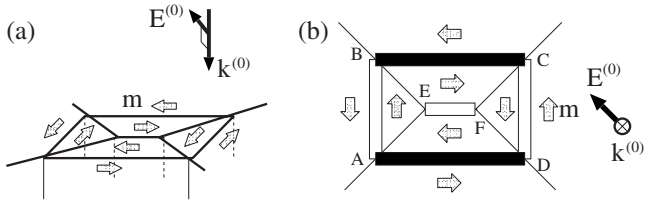

FIG. 1. (a) Schematic view of the experimental configuration (the Voigt configuration) of Fig. 2(b) in Schäfer *et al.* [5]. (b) Rotation angle pattern. The polarization vectors on the white and black lines rotate in opposite directions. The light is normally incident and linearly polarized with the polarization vector parallel to lines *BE* and *DF*. In this configuration, the FK effect disappears.

their experimental results is shown in Fig. 1. They pointed out the following characteristics of the SH effect for various materials:

(1) The rotation of the polarization vector due to the domain boundary survives under the Voigt configuration, which is a configuration that makes the FK effect disappear.

(2) The rotation angle is proportional to the magnitude of the magnetization, as in the FK effect.

(3) The rotation angle is independent of the internal wall structure.

(4) The rotation angle depends on the incident polarization vector while the FK effect does not.

Schäfer and Hubert [4] proposed a phenomenological formula to explain their experimental results. In addition to this formula, essentially two theoretical approaches have been proposed to take into account the gradient effect of magnetization. First, Schäfer and Hubert [4] modified the dielectric law, adding a term representing the magnetization gradient, and derived a formula for the rotation angle. The aim of this approach was to support the phenomenological formula on the basis of the gradient effect. Thiaville *et al.* [6] derived essentially the same formula using the isotropic fifth rank tensor. As I will indicate in Sec. V, the formula derived in these two papers is physically unacceptable because the rotation angle diverges in certain cases. The second approach relied on numerical methods for a system with nonuniform magnetization [7–9] based on the ordinary dielectric law, which leads to the FK effect. The numerical results matched the experimental results closely, but the physical explanation was obscured by the complicated calculations.

In short, no comprehensive physical explanation of the SH effect exists at the present time.

III. FORMULATION OF THE BOUNDARY MAGNETO-OPTICAL EFFECT

My theory in this section is based on the ordinary dielectric law with proper consideration of the domain boundaries. I previously introduced this method [10] to treat the optical near field of dielectric material.

I start with the dielectric law for a finite-sized material. Suppose a single magnetic domain occupies region $\mathcal{V}$ as shown in Fig. 2(a). In this system, the polarization $\mathbf{P}$ is defined as the product of the step function $\theta(\mathbf{r}\in\mathcal{V})$ and the polarization of the infinite-sized material $\mathbf{P}_\infty$,

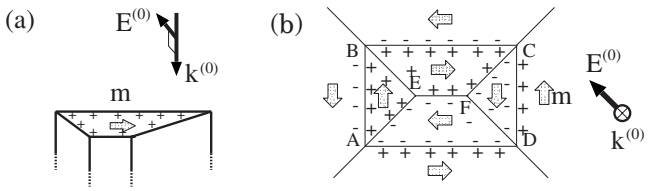

FIG. 2. Snapshot of the induced charge density of the boundary MOE at a certain time for systems with (a) one or (b) multiple magnetic domains (top view). The sign filling in the upper boundary of each domain is that of the BCF in Eq. (6).

$$\mathbf{P}(\mathbf{r},t) = \theta(\mathbf{r}\in\mathcal{V})\mathbf{P}_\infty(\mathbf{r},t), \tag{1}$$

$$\theta(\mathbf{r}\in\mathcal{V}) = \begin{cases} 1 & \text{for } \mathbf{r}\in\mathcal{V}, \\ 0 & \text{for } \mathbf{r}\notin\mathcal{V}. \end{cases}$$

$\mathbf{P}_\infty$ can be expressed as

$$\mathbf{P}_\infty(\mathbf{r},t) = (\epsilon_1-\epsilon_0)\mathbf{E}(\mathbf{r},t) + i\epsilon_1 Q\hat{\mathbf{m}}\times\mathbf{E}(\mathbf{r},t), \tag{2}$$

where ϵ_1 and ϵ_0 are the dielectric constant of the material and vacuum, respectively; Q is a parameter for the MOE and is proportional to the magnitude of the magnetization; and $\hat{\mathbf{m}}$ is the unit vector of the magnetization. The dielectric law in Eq. (1) is reasonable because it leads to the MBCs as I prove in Appendix A. See also [10] for the case of dielectric material.

Ignoring the dynamic magnetization, the induced charge density $\rho=-\nabla\cdot\mathbf{P}$ and the induced current density $\mathbf{j}=\partial_t\mathbf{P}$ are expressed as

$$\rho(\mathbf{r},t) = -\nabla\theta(\mathbf{r}\in\mathcal{V})\cdot\mathbf{P}_\infty(\mathbf{r},t) - \theta(\mathbf{r}\in\mathcal{V})\nabla\cdot\mathbf{P}_\infty(\mathbf{r},t), \tag{3}$$

$$\mathbf{j}(\mathbf{r},t) = \theta(\mathbf{r}\in\mathcal{V})\partial_t\mathbf{P}_\infty(\mathbf{r},t). \tag{4}$$

In Eqs. (3) and (4), the two terms containing θ constitute the bulk source and yield the bulk optical effect (FK effect) because these terms without the step function coincide with the source of the corresponding infinite-sized material. The term with $\nabla\theta$ is the boundary source (boundary charge density), because the factor $\nabla\theta(\mathbf{r}\in\mathcal{V})$ is the δ function, which represents localization at the boundary. The explicit expression of the boundary charge density is

$$\begin{aligned}\rho_{\text{boundary}}(\mathbf{r},t) &= -\nabla\theta(\mathbf{r}\in\mathcal{V})\cdot\mathbf{P}_\infty(\mathbf{r},t) \\ &= \int_{\partial\mathcal{V}} d^2s\,\delta^3(\mathbf{r}-\mathbf{s})\mathbf{n}_s\cdot[(\epsilon_1-\epsilon_0)\mathbf{E}(\mathbf{s}-0\mathbf{n}_s,t) \\ &\quad + i\epsilon_1 Q\hat{\mathbf{m}}\times\mathbf{E}(\mathbf{s}-0\mathbf{n}_s,t)],\end{aligned} \tag{5}$$

where $\partial\mathcal{V}$ is the boundary of region $\mathcal{V}$, $\mathbf{s}$ is the position vector on $\partial\mathcal{V}$, and $\mathbf{n}_s$ is the outward normal unit vector from $\mathbf{s}$. Equation (5) contains a singularity of the one-dimensional δ function, that is, the charge density is localized on the boundary surface and is responsible for MBCs as I prove in Appendix A. See also [10] for an elementary discussion of this issue. As discussed below, the term containing Q in the last form of Eq. (5) is the source of the boundary MOE, which is completely different from the bulk MOE (the FK effect).

As a result, based on a proper dielectric law, I derive and classify boundary and bulk MOEs on an equal footing. The source of the boundary effect is the boundary charge density, which is responsible for MBCs.

IV. SCHÄFER-HUBERT EFFECT AS A BOUNDARY EFFECT ORIGINATING FROM BOUNDARY CHARGE DENSITY

In this section, I show that the SH effect is the boundary effect originating from the boundary charge density derived in the preceding section. To understand the boundary optical effect in my theory intuitively, consider the simplest case as the first step; a single magnetic domain is exposed to normally incident, linearly polarized light as shown in Fig. 2(a). Since the bulk MOE (the FK effect) disappears in this configuration, the rotation is produced only by the MOE-related boundary charge density in Eq. (5). In the following, I will concentrate on the pattern of rotation, i.e., the white and black lines in Fig. 1(b). For this restricted purpose, it is sufficient to consider the next factor in Eq. (5). The last expression is called the boundary charge factor (BCF) in the following:

$$\mathbf{n}_s \cdot \hat{\mathbf{m}} \times \mathbf{E}(\mathbf{s} - 0\mathbf{n}_s, t) \sim \mathbf{n}_s \cdot \hat{\mathbf{m}} \times \mathbf{E}^{(0)} \exp(-i\omega t) \propto \mathbf{n}_s \cdot \hat{\mathbf{m}} \times \mathbf{E}^{(0)}, \quad (6)$$

where $\mathbf{E}^{(0)}$ is the incident polarization vector (constant vector) and ω is the incident angular frequency. The approximated formula on the right-hand side of Eq. (6) holds because the incident field possesses a common phase over the upper boundary under the Voigt configuration of Fig. 1. The BCF on the upper boundary is positive, while it is zero on the side boundary, that is, the MOE-related boundary charge density appears on the upper boundary. The charge compensating for the charge on the upper boundary is distributed diffusively in the bulk volume within the penetration depth due to the metallic property of the material.

In the case of a single domain, the charge on the upper boundary and its compensating charge form a dipole moment, which points in the direction normal to the upper boundary. Therefore, it does not radiate the scattered field in the direction normal to the upper boundary because the radiative field should be a transverse field.

Next, I consider a system with multiple magnetic domains as the combination of the simplest case mentioned above with an imaginary thin vacuum region between the neighboring domains; we treat Fig. 1(a). Here, I assume that the width of the domain wall is so small that the MOE of the domain wall itself is negligible. Let us focus on the upper boundary. The sign of BCF in Eq. (6) fills each area in the upper boundary of Fig. 2(b), which is a snapshot of the MOE-related boundary charge density at a certain time. The opposite signs appear in the pairs of domains across the lines *AB*, *BC*, *CD*, *AD*, *AE*, *EF*, and *CF*; that is, dipole moments appear across those lines. Here I implicitly assume that the width of the domain wall is smaller than the order of the light wavelength; if not, the present description using dipole moments is inadequate. Fortunately, this condition is roughly satisfied by Fig. 4 in [5]. This series of dipole moments oscillates at the same frequency as the incident light and radiates the scattered field in the direction normal to the upper boundary. Its polarization vector points in the same direction as the dipole moment, with three possible cases for the rotation.

(1) The polarization vector of the scattered field from lines *AE* and *CF* is parallel to the incident vector and does not lead to any rotation.

(2) Along lines *AB*, *CD*, and *EF*, the polarization vector rotates in a certain direction.

(3) In contrast, with respect to lines *BC* and *AD*, the polarization vector rotates in the direction opposite that in case (2).

Then, comparing Figs. 2(b) and 1(b), we find that the pattern of rotation based on this theory agrees with the experimental result.

Note the compensating charge. The material is metal with a thickness greater than the penetration depth, which is considered the effective thickness. Consequently, the compensating charge density forms a dipole moment across the domain boundary in the direction opposite that on the upper boundary. The far field is the superposition of the radiation field from the dipole moment on the upper boundary and that from the compensating dipole moment. The radiated field from the compensating source is partially absorbed by the metal bulk so that the contribution from the upper boundary survives.

Now, I confirm that my theory is consistent with the characteristics of the SH effect mentioned in Sec. II. As discussed above, the boundary MOE may appear when the bulk MOE (the FK effect) disappears, clarifying the first point. Although the bulk and boundary MOEs differ qualitatively, the two originate from the same dielectric law in Eq. (1) and are linearly dependent on Q. Since Q is proportional to the magnitude of the magnetization, the second point is satisfied. My theory does not require information on the internal wall structure, and thus the third point is clarified. For the dependence on the incident polarization vector, the boundary charge density based on the BCF in Eq. (6) almost completely explains the observed contrast as shown in the comparison chart in Fig. 3, so the last point is satisfied.

The comparison chart in Fig. 3 includes the results of my theory for 32 elementary configurations and the observed contrast for 18 configurations. In this chart, $\theta_{\text{this work}}$ is a factor proportional to the difference of the BCFs on the upper boundary between the two domains across the wall; see the next section for details. The sign of $\theta_{\text{this work}}$ based on the BCF in Eq. (6) can be easily checked using the same approach developed in Sec. III. To compare this theory, that is, $\theta_{\text{this work}}$, with the observed contrast in the 18 configurations, one configuration should be used to determine the overall sign of $\theta_{\text{this work}}$. Therefore, among the $17(=18-1)$ configurations observed, $15(=16-1)$ configurations match this theory, while two do not [13]. For these two exceptions, Kambersky *et al.* [8] proposed that they are due to a bulk effect originating from an underlying structure; see the next section for details.

Last, I estimate the order of rotation angle due to the boundary MOE using dimensional analysis. Although

Elementary Configuration No.	$\mathbf{m}_1$	$\mathbf{m}_2$	$\mathbf{E}^{(0)}$	ω	α	γ	Observed Contrast B/W	Refs.	$\theta_{\text{this work}}$	θ_{SH}	θ_{SHT}	Kambersky et al. [f]
1	⇗	⇘	→	$\pi/2$	$\pi/4$	$-\pi/4$	W	a	$\sqrt{2}/4$	$\sqrt{2}/2$	$\sqrt{2}/2$	–
2					$\pi/2$	0	0		0	0	div.	–
3					$3\pi/4$	$\pi/4$	B		$-\sqrt{2}/4$	$-\sqrt{2}/2$	$-\sqrt{2}/2$	–
4					π	$\pi/2$	0		0	0	div.	–
5	⇖	⇖	→		$-3\pi/4$	$-\pi/4$	B	a,d	$-\sqrt{2}/4$	$-\sqrt{2}/2$	$-\sqrt{2}/2$	–
6					$-\pi/2$	0	0		0	0	div.	–
7					$-\pi/4$	$\pi/4$	W		$\sqrt{2}/4$	$\sqrt{2}/2$	$\sqrt{2}/2$	–
8					0	$\pi/2$	0		0	0	div.	–
9	⇗	⇖	→		$-\pi/4$	$-\pi/4$	–		$-\sqrt{2}/4$	0	0	–
10					0	0	–		0	$\sqrt{2}/2$	indet.	–
11					$\pi/4$	$\pi/4$	–		$-\sqrt{2}/4$	0	0	–
12					$\pi/2$	$\pi/2$	–		$-\sqrt{2}/2$	$-\sqrt{2}/2$	indet.	–
13	⇗	⇘	→		$3\pi/4$	$-\pi/4$	–		$\sqrt{2}/4$	0	0	–
14					π	0	–		0	$-\sqrt{2}/2$	indet.	–
15					$-3\pi/4$	$\pi/4$	–		$\sqrt{2}/4$	0	0	–
16					$-\pi/2$	$\pi/2$	–		$\sqrt{2}/2$	$\sqrt{2}/2$	indet.	–
17	⇧	⇩	→	π	$\pi/4$	$-\pi/4$	W	a,d	1/2	1	1	B
18					$\pi/2$	0	0		0	0	div.	–
19					$3\pi/4$	$\pi/4$	B		−1/2	−1	−1	W
20					π	$\pi/2$	0		0	0	div.	–
21	⇩	⇧	→		$-3\pi/4$	$-\pi/4$	B	a,b,c,d	−1/2	−1	−1	W
22					$-\pi/2$	0	0		0	0	div.	–
23					$-\pi/4$	$\pi/4$	W		1/2	1	1	B
24					0	$\pi/2$	0		0	0	div.	–
25	⇨	⇦	→		$-\pi/4$	$-\pi/4$	–	e	−1/2	0	0	–
26					0	0	B		0	1	indet.	0
27					$\pi/4$	$\pi/4$	–		−1/2	0	0	–
28					$\pi/2$	$\pi/2$	–		−1	−1	indet.	W
29	⇦	⇨	→		$3\pi/4$	$-\pi/4$	–	e	1/2	0	0	–
30					π	0	W		0	−1	indet.	0
31					$-3\pi/4$	$\pi/4$	–		1/2	0	0	–
32					$-\pi/2$	$\pi/2$	–		1	1	indet.	B

FIG. 3. Comparison chart for the results of experiments, my theory and other theories for 32 elementary configurations. For the contrast representing the rotation angle, "B," "W," "0," and "–" stand for the "black line," "white line," "background level," and "configuration of no appearance," respectively. The abbreviations "div" and "indet" indicate divergence and indeterminate form, respectively. The contrasts of experimental and theoretical studies are from the following references: (a) Figs. 4(d) and 4(f) for silicon iron in [4]; (b) Fig. 2(b) for silicon iron in [5]; (c) Fig. 5(b) for iron permalloy in [5]; (d) Figs. 1(a), 1(b), 1(c), and 1(d) for silicon iron in [6]; (e) Fig. 2(a) for iron-rich metallic glass in [6]; and (f) Figs. 8(a) and 8(b) in [8] (theory).

Schäfer *et al.* [4,5] used silicon iron and other multicomponent materials, I use iron because I could not obtain detailed information about their samples. From [11], the Faraday rotation for iron is $F=4.4\times10^5$ deg/cm at a wavelength in a vacuum of $2\pi/k^{(0)}=500$ nm. The rotation angle due to the bulk MOE (the FK effect) is estimated as $\theta_{\text{FK}}=Fa=F/k^{(0)}[k^{(0)}a]^1$, where a is the path length of the light. For dimensional analysis, the nondimensional quantity θ_{FK} is expressed in terms of two nondimensional quantities $F/k^{(0)}$ and $k^{(0)}a$, which characterize the system. In practice, the bulk MOE of iron is observed as the Kerr rotation $\theta_{\text{FK}}\sim1°$ [14]. The boundary effect should carry one path length less relative to the bulk effect. Therefore, the rotation angle due to the boundary MOE (the SH effect) originating from the boundary charge density on the upper boundary is roughly estimated as $\theta_{\text{boundary MOE}}=F/k^{(0)}[k^{(0)}a]^0\sim4°$. This rotation angle for the SH effect is the same order as θ_{FK} and detectable by Kerr optics. We must ensure that the real rotation angle of the boundary MOE is smaller than 4° because this rotation is partially canceled by the effect of the compensating charge density. Indeed, the experiments by Schäfer *et al.* indicated that $\theta_{\text{FK}}>\theta_{\text{boundary MOE}}$.

Altogether, this theory explains the experimental results fairly well, so that the SH effect is the boundary effect derived in my theory, accompanied by the bulk effect (FK effect), and originates from the boundary charge density.

V. COMPARISON WITH OTHER THEORIES

In this section, I compare my theory with others. Figure 3 shows a comparison chart for 32 elementary configurations, which summarizes the results of experiments, my theory and other theories. The configurations shown in the insets of Fig. 3 can be parametrized by the three specific angles ω, α, and γ that are introduced in [4]; the notation for ω, α, and γ is given in Fig. 4(a), assuming that the incident light is polarized linearly and normal to the upper boundary.

First, I compare my theory with the phenomenological formula proposed by Schäfer and Hubert [4],

$$\theta_{\text{SH}} \propto \sin\frac{\omega}{2}\cos(\alpha+\gamma). \tag{7}$$

In my theory, the boundary charge density on the upper boundary of each domain is proportional to the BCF in Eq.

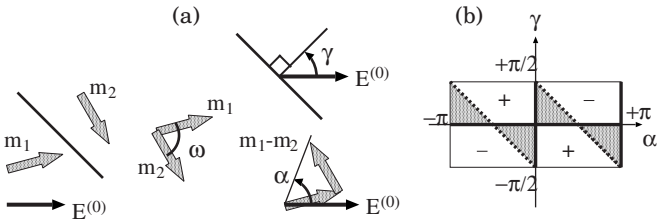

FIG. 4. (a) The notation for three specific angles: $\omega \in [0,\pi]$ is the absolute value of the angle between the two magnetization vectors, namely, $\mathbf{m}_1$ and $\mathbf{m}_2$. $\gamma \in (-\pi/2,\pi/2]$ is the orientation angle of the domain wall normal vector relative to $\mathbf{E}^{(0)}$, while the normal vector is outward from the first to the second domain. If $\gamma \notin (-\pi/2,\pi/2]$, exchange the labels "1" and "2" for the magnetization of the two domains. $\alpha \in (-\pi,\pi]$ is the orientation angle of $\mathbf{m}_1 - \mathbf{m}_2$ relative to $\mathbf{E}^{(0)}$. One can define $\mathbf{E}^{(0)}$ in the opposite direction; time-averaged experimental results including those for MOEs should not be affected by this change. Indeed, we obtain the same angles ω, α, and γ as the original ones because we need to exchange the labels of the two domains to satisfy $\gamma \in (-\pi/2,\pi/2]$. (b) (α,γ) parameter space. In the bright area, Eq. (7) and Eq. (8) take the common sign shown, while in the dark area, they take the opposite sign. The dotted and thick lines are the nodal lines of Eq. (7) and Eq. (8), respectively.

(6). Therefore, along the domain wall, the amplitudes of the dipole moment and the scattered field are scaled by the difference of those two BCFs, that is, $\mathbf{n}_s \cdot (\hat{\mathbf{m}}_2 - \hat{\mathbf{m}}_1) \times \mathbf{E}^{(0)} \propto \sin\frac{\omega}{2}\sin\alpha$, and the scattered polarization vector is normal to the domain wall. Suppose the x axis is directed to $\mathbf{E}^{(0)}$ and the z axis is directed to the boundary normal of the upper surface. Then the y component of the scattered field is proportional to the rotation angle under the weak scattering condition, resulting in

$$\theta_{\text{this work}} \propto -\sin\frac{\omega}{2}\sin\alpha\sin\gamma. \tag{8}$$

Under the condition that $\cos\alpha\cos\gamma = 0$, Eq. (8) is identical to Eq. (7). Even if this condition is not satisfied, Eq. (7) and Eq. (8) have the same sign in most cases that belong to the bright area in Fig. 4(b). Indeed, throughout the 16 configurations numbered 1–8 and 17–24, Eqs. (7) and (8) are essentially the same, aside from a constant factor. For other configurations, see the last part of this section.

Schäfer and Hubert [4] proposed another formula employing tensor analysis with the aim of supporting Eq. (7) using the gradient effect of magnetization. Thiaville *et al.* [6] subsequently derived essentially the same formula in a more precise manner using the isotropic fifth rank tensor. They modified the dielectric law, adding a term to include the gradient of magnetization, and derived the formula in the right-hand side of the next equation,

$$\theta_{\text{SHT}} \sim -\frac{\partial m_x}{\partial x} + \frac{\partial m_y}{\partial y} \propto -\sin\frac{\omega}{2}\frac{\sin(\alpha-\gamma)}{\sin 2\gamma}. \tag{9}$$

The right-hand side is expressed in terms of the three specific angles; see Appendix B for the derivation. The last expression of Eq. (9) has a singularity at $\gamma = 0, \frac{\pi}{2}$, that is, a large rotation angle appears if the polarization of light is set to $\gamma = 0, \frac{\pi}{2}$. However, the experimental results in the configurations numbered 2, 4, 6, 8, 18, 20, 22, and 24 do not support this. Therefore, Eq. (9) is physically unacceptable, although it coincides with Eq. (7) except for the configurations with $\gamma = 0, \frac{\pi}{2}$ in Fig. 3.

Using a different approach, numerical methods for a system with inhomogeneous magnetization were developed [7–9]. These theories treated the gradient effect of magnetization based on the familiar dielectric law leading to the FK effect. The last column in Fig. 3 is the result of Kambersky *et al.* [8] and qualitatively coincides with my theory except for the overall sign. Although their papers showed fewer figures of contrast patterns, my theory is expected to be compatible with theirs because both theories are based on essentially the same dielectric law. The boundary effect in my theory is considered as a limit of the gradient effect of magnetization in the small width of the domain wall. The difference is that they essentially used MBCs to perform quantitative calculations for systems with inhomogeneous magnetization, while my work uses boundary charge density to extract the essence of the SH effect from the perspective of general boundary optical effects.

The remaining work in this section is to determine the experimental configurations in which my theory produces different results from other theories. My theory and the theories for inhomogeneous magnetization are expected to produce the same contrast patterns, and the tensor method represented by Eq. (9) is physically excluded. Therefore, it is sufficient to compare Eq. (7) for θ_{SH} and Eq. (8) for $\theta_{\text{this work}}$ in Fig. 3. The differences between the two formulas appear in the configurations numbered 9–11, 13–15, 25–27, and 29–31. All these are configurations with head-on-like magnetization and are located on the two types of nodal lines in the (α,γ) parameter space in Fig. 4(b). Unfortunately, the head-on-like magnetization in a simple domain structure does not appear in the literature of experimental results in [4–6]. Perhaps this is due to the instability of the head-on-like domain structures, which possess excess magnetostatic energy of the domain wall. Exceptionally, the experimental results for configurations 26 and 30 are reported. However, neither of the two theories is compatible with the observed contrast, if the meaning of "B" and "W" is common in the series of experimental results listed in Fig. 3. See also [13] in Sec. IV. Kambersky *et al.* [8] pointed out that in these configurations, the magnetization gradient brings about no rotation as in my theory, and proposed that the experimental result is due to the bulk effect originating from an underlying structure that decreases the excess magnetostatic energy of the domain wall of the head-on magnetization.

To check these theories, more experimental results are required in the configurations with the head-on-like magnetization. Furthermore, comparing not only the signs but also the magnitudes of Eqs. (7) and (8) with the observed rotation angle is warranted.

VI. SH EFFECT IN NEAR-FIELD OPTICS

The SH effect was observed in the far field of systems with large-scale domains under conditions in which the FK

effect is extinguished. In addition to this experimental condition, I predict that the SH effect is dominant and detectable in the near field of a system with small-scale domains. The following discussion is based on dimensional analysis.

Consider a magneto-optical system with small-scale domains of arbitrary magnetization and with an oblique incidence. The linear scale a of the domain is smaller than the order of the light wavelength $2\pi/k^{(0)}$, so that $k^{(0)}a \lesssim 1$ is satisfied. Such a situation is required by high bit-density MO storage. The fundamental physical principle mentioned in Sec. I tells us that the boundary effect in such a system predominates over the bulk effect. We ensure that the bulk source in the volume of a domain carries one more length dimension than the boundary source on the surface of a domain. Indeed, if the rotation angle of the FK effect is of the order a^n, or $[k^{(0)}a]^n$ in nondimensional form, for $n \geq 1$, then that of the SH effect should be of the order a^{n-1}, or $[k^{(0)}a]^{n-1}$. Therefore, if the scale a is sufficiently small, then the boundary MOE dominates the bulk MOE. To detect the SH effect in such a small-scale system, a near-field optical technique is essential to distinguish the rotations due to the neighboring domain walls, as mentioned in Sec. I.

As a result, the SH effect should be the dominant MOE in a small-scale system and will be observed in near-field optics.

VII. SUMMARY

In conclusion, I derived and classified boundary and bulk MOEs concurrently from a familiar dielectric law. The bulk effect is the FK effect, while the boundary effect is identified to the SH effect. Although the dielectric law in this theory is not a new one, the present theory uses boundary charge density and gives a clear physical explanation of the SH effect or the gradient effect of magnetization developed by the pioneers. In short, I presented evidence of a boundary MOE driven by the boundary charge density. Furthermore, I pointed out that the SH effect predominates over the FK effect in a system with small-scale domains and is detectable in near-field optics.

My theoretical scheme leads to the boundary and bulk effects concurrently and is expected to be effective not only for the MOE but also for various other effects, replacing Eq. (2). Therefore, the SH effect is a member of a family of boundary optical effects driven by boundary charge density. In another presentation, it will be shown in a general manner that such boundary effects are dominant in a system of near-field optics.

ACKNOWLEDGMENTS

I thank Professor Kazumi Fujima of the University of Yamanashi, Kofu City, Japan, for his critical review of this paper and Professor Hirokazu Hori of the same university for his valuable advice.

APPENDIX A: BOUNDARY CHARGE DENSITY AND MAXWELL'S BOUNDARY CONDITIONS

Here I prove that both Eq. (1) and Eq. (5) lead to MBCs, so that my theory is compatible with ordinary classical optics, e.g., [7–9]. Ordinary optics and my theory both ignore dynamic magnetization. Therefore, all components of the magnetic field in light are continuous across the boundary surface. In addition, the surface-parallel component of the electric field is always continuous because it is derived from Faraday's law, which is independent of the charge and current density. Therefore, I focus on the boundary condition for the surface-normal component of electric field which is derived from Coulomb's law,

$$\nabla \cdot \mathbf{E}(\mathbf{r},t) = \frac{-1}{\epsilon_0} \nabla \cdot [\theta(\mathbf{r} \in \mathcal{V})\mathbf{P}_\infty(\mathbf{r},t)]. \tag{A1}$$

Consider a boundary element of which the normal vector is directed to the x axis, that is, $\mathbf{n}_s = \mathbf{x}$ and a volume element that includes the boundary element and an infinitesimal width across the domain wall. The position vector on the boundary element is $\mathbf{s}$ and it is assumed that $\mathbf{s}+0\mathbf{x}$ and $\mathbf{s}-0\mathbf{x}$ belong to the vacuum and material regions, respectively, and are located on the boundary surface of the thin volume element. Integrating over this volume element and employing Gauss's theorem produces the next boundary condition,

$$\mathbf{x} \cdot \mathbf{E}(\mathbf{s}+0\mathbf{x},t) - \mathbf{x} \cdot \mathbf{E}(\mathbf{s}-0\mathbf{x},t) = \frac{1}{\epsilon_0}\mathbf{x} \cdot \mathbf{P}(\mathbf{s}-0\mathbf{x},t). \tag{A2}$$

If we move the second term on the left-hand side to the right-hand side, Eq. (A2) represents the well-known boundary condition indicating that the surface-normal component of the displacement vector field $\epsilon_0\mathbf{E}(\mathbf{r},t)+\mathbf{P}(\mathbf{r},t)$ is continuous across the boundary surface. Therefore, Eq. (1) is compatible with ordinary classical optics.

Next let us examine Coulomb's law using the boundary charge density of Eq. (5),

$$\nabla \cdot \mathbf{E}(\mathbf{r},t) = \frac{1}{\epsilon_0}\left(\int_{\partial\mathcal{V}} d^2s\, \delta^3(\mathbf{r}-\mathbf{s})\mathbf{n}_s \cdot \mathbf{P}_\infty(\mathbf{s}-0\mathbf{n}_s,t) - \theta(\mathbf{r} \in \mathcal{V})\, \nabla \cdot \mathbf{P}_\infty(\mathbf{r},t) \right). \tag{A3}$$

Integrating Eq. (A3) over the volume element, applying Gauss's theorem to the left-hand side, and considering that the second term on the right-hand side vanishes in the integration over the infinitesimal section along the x axis, this simply reduces to Eq. (A2). Therefore, Eq. (5) is properly responsible for MBCs.

APPENDIX B: EXPRESSION FOR θ_{SHT} IN TERMS OF SPECIFIC ANGLES

Suppose that the change in the magnetization is $\Delta\mathbf{m} = \mathbf{m}_2 - \mathbf{m}_1$ across the boundary with the width d and set x axis, y axis, and $\mathbf{E}^{(0)}$ are included in the upper boundary; the

direction of the x axis is that of $\mathbf{E}^{(0)}$. If $|\mathbf{m}_2|=|\mathbf{m}_1|=m$, then $|\Delta\mathbf{m}|=2m\sin(\omega/2)$, $\Delta\mathbf{m}_x=|\Delta\mathbf{m}|\cos\alpha$, and $\Delta\mathbf{m}_y=|\Delta\mathbf{m}|\sin\alpha$. Then, the change of position across the boundary wall is $\Delta x=d\cos\gamma$ and $\Delta y=d\sin\gamma$, so that in the limit of small width of the domain wall, Eq. (9) results in

$$\theta_{\mathrm{SHT}} \sim -\frac{\partial m_x}{\partial x}+\frac{\partial m_y}{\partial y} \simeq \frac{2m}{d}\sin\frac{\omega}{2}\left(-\frac{\cos\alpha}{\cos\gamma}+\frac{\sin\alpha}{\sin\gamma}\right) = \frac{4m}{d}\sin\frac{\omega}{2}\frac{\sin(\alpha-\gamma)}{\sin 2\gamma}. \tag{B1}$$

[1] M. Faraday, *Experimental Researches in Electricity* (Dover, New York, 1965), series 19.

[2] S. Tsunashima, J. Phys. D **34**, R87 (2001).

[3] E. Betzig and J. K. Trautman, Science **257**, 189 (1992); E. Betzig, J. K. Trautman, R. Wolfe, E. M. Gyorgy, P. L. Finn, M. H. Kryder, and C.-H. Chang, Appl. Phys. Lett. **61**, 142 (1992); E. Betzig, J. K. Trautman, J. S. Weiner, T. D. Harris, and R. Wolfe, Appl. Opt. **31**, 4563 (1992).

[4] R. Schäfer and A. Hubert, Phys. Status Solidi A **118**, 271 (1990).

[5] R. Schäfer, M. Rührig, and A. Hubert, IEEE Trans. Magn. **26**, 1355 (1990).

[6] A. Thiaville, A. Hubert, and R. Schäfer, J. Appl. Phys. **69**, 4551 (1991).

[7] V. Kambersky, J. Magn. Magn. Mater. **104–107**, 311 (1992).

[8] V. Kambersky, L. Wenzel, and A. Hubert, J. Magn. Magn. Mater. **189**, 149 (1998), and references therein.

[9] G. Traeger, L. Wenzel, and A. Hubert, IEEE Trans. Magn. **29**, 3408 (1993).

[10] I. Banno, in *Progress in Nano-Electro-Optics II*, edited by M. Ohtsu (Springer, Berlin, 2004), p.1.

[11] *CRC Handbook of Chemistry and Physics*, 87th ed. (CRC, Boca Raton, FL, 2006), Chap. 12.

[12] In this paper, the difference between the Faraday and Kerr effects is not important, so that I unify the two and state as the Faraday-Kerr effect.

[13] For the observed contrasts in the comparison chart in Fig. 3, the meaning of "B" (black) and "W" (white) seems to be common across the five sets of experimental results labeled (a)–(e), even independently of sample materials. However, just to check, suppose an inopportune situation in which the setup and the sample of every set of experiments affect the notation of "B/W." Then, one configuration with "B" or "W" in every set of experimental results [except that with label (e)] should be used to determine the overall sign factor of $\theta_{\text{this work}}$, so that the statement becomes "Among 14(=18−4) configurations, 12(=16−4) configurations match." Even in this situation, my theory is still supported by the experimental results.

[14] For an order estimation of Kerr rotation, consider a system with both the magnetization and incidence normal to the upper boundary. In this system, the path length a is considered as to be 2 times the penetration depth, over which the light travels to and from the iron bulk. The penetration depth is the reciprocal of the absorption coefficient, which is 6.5×10^5 cm^{-1} for iron [11]. Therefore, the path length is $a=31$ nm, giving $\theta_{\mathrm{FK}}=Fa\sim1°$.